ACS Chemical Neuroscience

pubs.acs.org/chemneuro

Research Article

α_1 Subunit Histidine 55 at the Interface between Extracellular and Transmembrane Domains Affects Preactivation and Desensitization of the $GABA_A$ Receptor

Przemyslaw T. Kaczor,* Aleksandra D. Wolska, and Jerzy W. Mozrzymas*

Cite This: *ACS Chem. Neurosci.* 2021, 12, 562−572

Read Online

ACCESS | Metrics & More | Article Recommendations

ABSTRACT: The $GABA_A$ receptor is a member of the Cys-loop family and plays a crucial role in the adult mammalian brain inhibition. Although the static structure of this receptor is emerging, the molecular mechanisms underlying its conformational transitions remain elusive. It is known that in the Cys-loop receptors, the interface between extracellular and transmembrane domains plays a key role in transmitting the "activation wave" down to the channel gate in the pore. It has been previously reported that histidine 55 (H55), located centrally at the interfacial $\beta1-\beta2$ loop of the α_1 subunit, is important in the receptor activation, but it is unknown which specific gating steps it is affecting. In the present study, we addressed this issue by taking advantage of the state-of-the-art macroscopic and single-channel recordings together with extensive modeling. Considering that H55 is known to affect the local electrostatic landscape and because it is neighbored by two negatively charged aspartates, a well conserved feature in the α subunits, we considered substitution with negative (E) and positive (K) residues. We found that these mutations markedly affected the receptor gating, altering primarily preactivation and desensitization transitions. Importantly, opposite effects were observed for these two mutations strongly suggesting involvement of electrostatic interactions. Single-channel recordings suggested also a minor effect on opening/closing transitions which did not depend on the electric charge of the substituting amino acid. Altogether, we demonstrate that H55 mutations affect primarily preactivation and desensitization most likely by influencing local electrostatic interactions at the receptor interface.

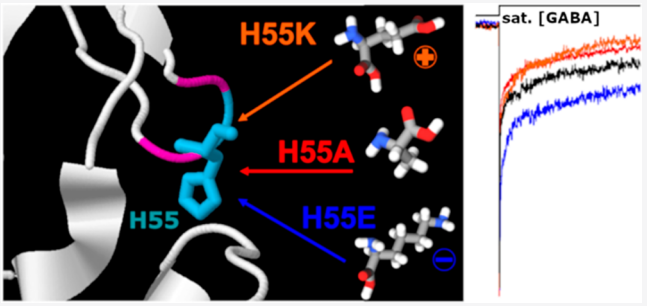

KEYWORDS: *Structure−function relationship, electrostatic interaction, Cys-Loop receptor, gating, histidine, patch clamp*

INTRODUCTION

Cys-loop receptors form a large family of pentameric, cation or anion selective receptors.[1] $GABA_A$ receptors ($GABA_ARs$) belong to this superfamily and play a crucial inhibitory role in the adult mammalian brain.[2,3] $GABA_ARs$ are a target for many endogenous compounds such as neurosteroids[4] or endozepines,[5] and for multiple exogenous pharmacological agents, many of them are of clinical relevance, such as anesthetics, benzodiazepines, and barbiturates.[6−10] The structure of Cys-loop receptors and of $GABA_ARs$, in particular, has been intensely studied, and several important reports on $GABA_ARs$' static structure have recently appeared.[11−16] However, the molecular mechanisms underlying the receptor activation remain elusive. It is of note that since the ligand binding site (LBS) located at the extracellular domain (ECD)[17] and the channel gate at the channel pore are particularly distant (approximately 50 Å), the transduction of the activation signal to the receptor gate is most likely very complex and awaits further investigations. Importantly, various residues located at the binding site or its close vicinity were found to affect not only agonist binding but also the receptor gating, occurring at later stages of the receptor activation.[18−23] This suggests that structural determinants of various stages of receptor gating are not spatially segregated and compartmentalized, but rather, the functioning of the receptor macromolecule is determined by long-range interactions leading to its cooperative mode of action. Studies on other Cys-loop receptors than $GABA_ARs$ as well as on some related bacterial channels indicated that that the interface between the ECD and the transmembrane domain (TMD) is crucial in transferring signal down to the channel gate.[24−27] In the case of $GABA_ARs$, the importance of this interface has been indicated by many groups.[28−30] In particular, Kash and coworkers[29] observed that the mutation of histidine H55 at the

Received: December 7, 2020
Accepted: January 13, 2021
Published: January 20, 2021

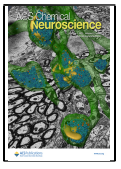

α_1 subunit (loop connecting β1 and β2 strands at the ECD) affected the dose−response relationship for GABA. However, it remains unknown which specific conformational transitions involved in the receptor gating are affected by mutations of this residue. An important feature of histidine is its complex electrostatics related primarily to interactions with its imidazole ring that are responsible, for instance, for proton shuttle mechanisms found, for example, in the active center of Carbonic Anhydrase II.[31,32] This electrostatic context of histidine is additionally interesting considering the fact that H55 is located between two negatively charged residues (aspartates in the case of the α_1 subunit) which are strongly conserved through the α subunit family (Figure 1). The

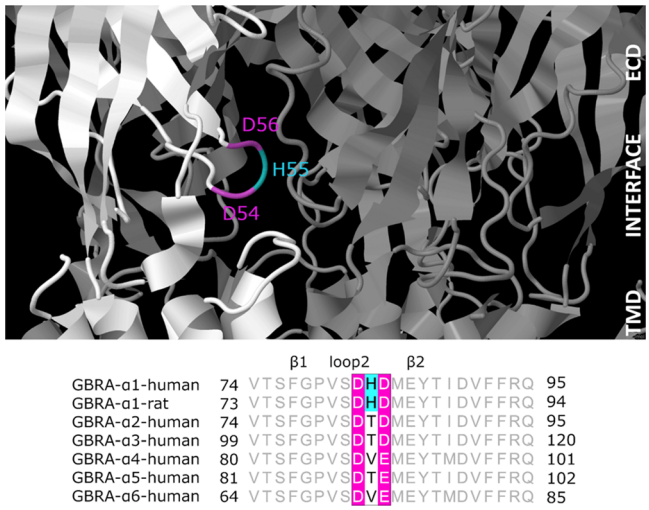

Figure 1. $GABA_A$ receptor TMD−ECD interface structure and alignment of Loop2 in α subunits. The α_1 subunit is marked with white/light gray colors, and the H55 residue on Loop 2 is indicated with cyan and neighboring aspartates−with magenta. Loop 2, between β1 and β2 strands of α_1 and other α subunits, is located at the interface between the ECD and TMD. The alignment of different α subunits reveals that in the center of loop 2 there is a highly conserved motive of two negatively charged residues separated with an amino acid (in α_1-histidine H55) showing different electrostatic properties. Structure visualization based on the $GABA_AR$ structure is obtained by ref 11.

physicochemical features of histidine are making this amino acid very interesting in the context of molecular architecture of the macromolecules. In particular, histidine may play an important role at many critical locations (e.g., the ECD−TMD interface) not only within specific subunits but also in the intersubunit and protein interactions. Considering thus the importance of the ECD−TMD interface in the receptor activation and a strategic position of H55, we have addressed the specific role of this residue in $\alpha_1\beta_2\gamma_{2L}$ $GABA_AR$ gating transitions. In this context, it is important to emphasize that recent functional studies on $GABA_ARs$[18,33,34] indicated that gating of this receptor is a process considerably more complex than previously believed, consisting of several conformational transitions, and some of them, e.g., flipping/preactivation, have been only recently described in these receptors. We thus decided to take advantage of the state-of-the-art kinetic analysis of $GABA_ARs$ toward the goal to explore the role of the H55 residue in the functioning of this receptor. Considering the specific electrostatic environment of H55, we have substituted this residue with glutamic acid and with lysine. In the context of local electrostatics, it is worthwhile to refer to respective pK_a values. For histidine, it is 6.04 which is relatively close to pH = 7.2, and it is generally assumed that in physiological conditions this amino acid is "partially" charged, i.e., only a fraction of these residues carries a net positive charge. For glutamate and lysine, pK_a values are 4.15 and 10.67, respectively, and at physiological pH, it is assumed that these residues carry stably negative and positive charges, respectively. It is noteworthy, however, that these values are determined in aqueous solutions, and pK_a for amino acids embedded in polypeptide chains within a macromolecule might show some differences. In addition, to shed light on the possible importance of steric interactions, a substitution with a small neutral amino acidic alanine was also considered. Our macroscopic and single-channel recordings together with extensive modeling have demonstrated that the H55 mutation resulted primarily in altering flipping/preactivation and desensitization transitions with some minor effects also on opening/closing. H55 substitutions with lysine and glutamate tended to produce opposite effects underscoring the importance of local electrostatic interactions.

RESULTS AND DISCUSSION

Impact of the α_1H55 Mutation on Macroscopic Responses. The effect of the considered mutations on receptor functioning was first assessed for agonist potency by determining the dose−response relationships (Figure 2).

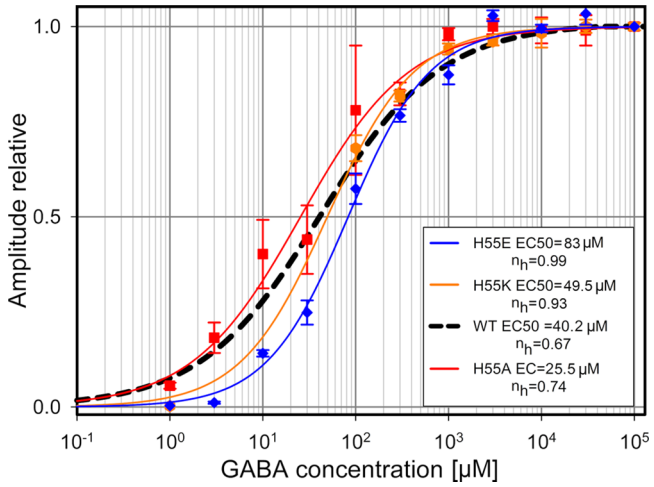

Figure 2. Dose−response studies reveal little impact of H55 mutations on agonist potency. Comparison of normalized (to current amplitude determined for saturating [GABA], sufficient for saturation for all mutants, on the same cell) dose−response relationships for H55 mutants to that for WT receptors fitted with Hill's eq 5. In the case of WT, the relationship (black dashed curve) was determined in our previous study.[35]

Whereas lysine mutation had practically no effect (EC50 = 49.5 μM, for WT EC50 = 40.2 μM), in the case of the glutamate mutant, a small rightward shift was observed (EC50 = 83 μM). Interestingly, a relatively minor leftward shift was seen (EC50 = 25.5 μM) for the alanine mutant. Thus, for all mutants and WT receptors, [GABA] of 10 mM was sufficient to ensure saturation.

Next, to get insight into the impact of H55 mutations on receptor gating, we analyzed the kinetics of current responses elicited by saturating [GABA] (10 mM) for the mutants and

https://dx.doi.org/10.1021/acschemneuro.0c00781
ACS Chem. Neurosci. 2021, 12, 562−572

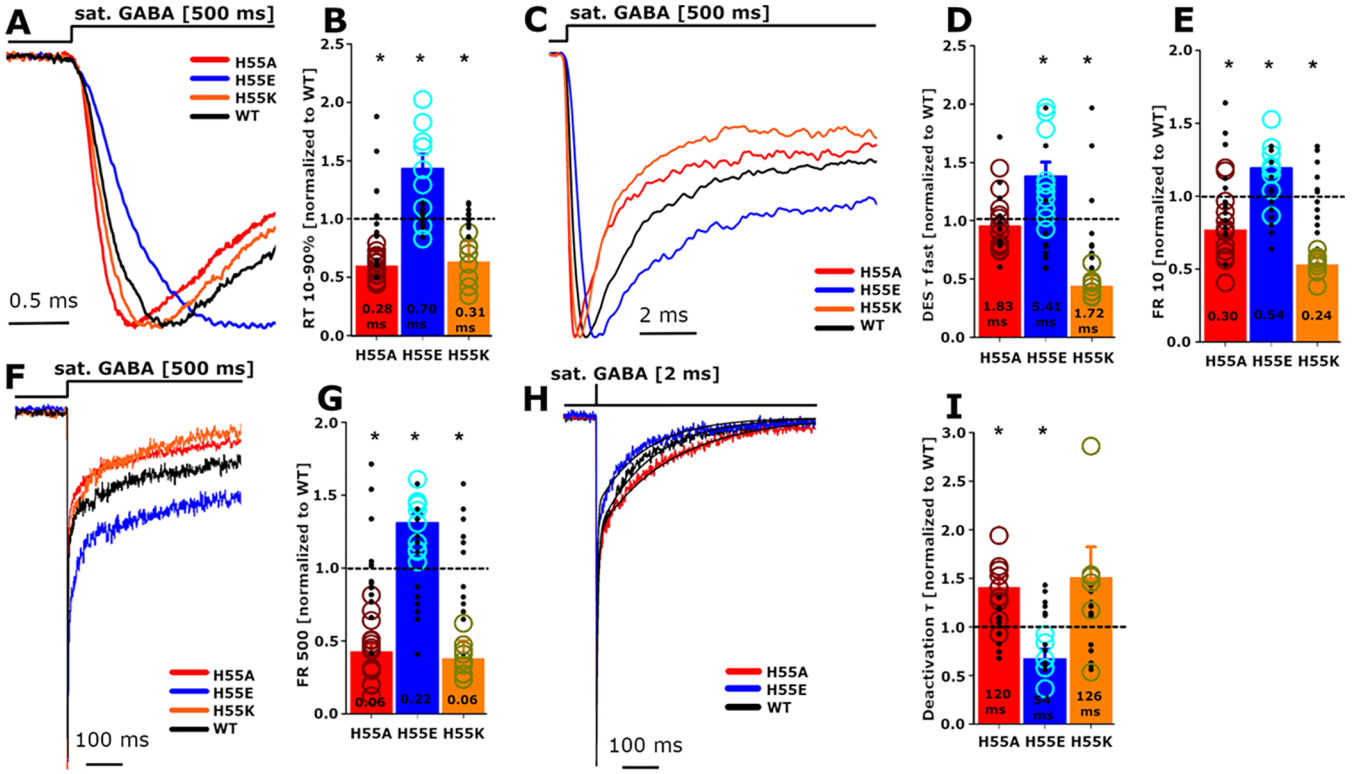

Figure 3. H55 mutations affect the time course of macroscopic currents evoked by saturating [GABA]. Normalized current traces showing the onset kinetics for WT (black), H55A (red), H55K (orange), and H55E (blue). (B) Statistics for the rise time (RT) values for H55 mutants, relative to RT values for WT receptors (see Materials and Methods). (C) Normalized traces of current responses to prolonged applications of saturating [GABA], revealing differences in the rate and extent of the rapid component of macroscopic desensitization. (D) and (E) show the statistics for the relative change in the desensitization time constant and FR10 parameter, respectively. (F) Normalized current responses to long applications of saturating [GABA] showing biphasic desensitization onset. (G) Statistics for the FR500 parameter. (H) Normalized current traces elicited by short (2 ms) applications of GABA displaying the time course of the deactivation process. Black lines represent fits with a sum of two exponential functions (eq 2). (I) Statistics for the relative mean deactivation time constants for H55 mutants. At the bottom of each bar the mean absolute value for a given parameter is disclosed. Insets above current traces indicate GABA applications, and asterisks indicate significant changes with respect to the controls (WT).

WT receptors. To ascertain the highest possible resolution, this set of experiments was performed in the outside-out patch configuration, at which the exchange time is the most rapid. An important feature of the receptor is the maximum speed of activation which can be observed upon application of saturating [GABA]. When H55 was substituted with a negatively charged glutamate (H55E), the current onset (RT, 10%−90%) was significantly prolonged with respect to the WT receptors (H55E: 0.7 ± 0.06 ms, n = 10, WT: 0.49 ± 0.01 ms, n = 11, p = 0.002). Interestingly, when substituting H55 with positively charged lysine (H55K), the opposite effect was observed (H55K: 0.31 ± 0.09 ms n = 9, p = 0.001). Moreover, when substituting H55 with small and neutral alanine (H55A), a similar RT shortening was observed as in the case of lysine (H55A: 0.28 ± 0.01 ms, n = 15, WT: 0.48 ± 0.05 ms, n = 13, p = 0.003, Figure 3A, Figure 3B). These results clearly indicate that H55 is involved in shaping the receptor gating. To pursue this issue, we have examined the time course of the macroscopic desensitization in responses elicited by prolonged (500 ms) applications of saturating [GABA] (Figure 3C). To visualize the kinetics and extent of desensitization at various time windows, the rapid time constant (DES τ fast) and FR10 and FR500 (percentages of currents, respectively 10 and 500 ms after the peak) parameters were calculated. Considering that the desensitization time course was at least biphasic, we found the use of FR parameters the most consistent. In the case of WT receptors and all considered mutants, a very pronounced rapid desensitization component was observed (Figure 3C). As presented in Figure 3D, substitution with glutamate resulted in a significant slowdown of this desensitization time constant (DES τ fast, H55E: 5.41 ± 0.5 ms, n = 10, WT: 3.91 ± 0.05 ms, n = 11, p = 0.022), but substitution with lysine resulted in an opposite effect (H55K: 1.72 ± 0.12 ms, n = 9, p = 0.001), similar to what was observed in the RT analysis. However, the H55 mutation to alanine (H55A) did not influence significantly this desensitization component. In the cases of the FR10 and FR500 parameters, H55 substitution to glutamate (H55E) or to lysine (H55K) resulted in opposite effects (Figure 3E−3G). In addition, H55A substitution resulted in a similar decrease in FR parameters as in the case of lysine (Figure 3E−3G). We have additionally analyzed the time course of deactivation (current relaxation following agonist removal) for short (2 ms) saturating [GABA] applications, which are believed to reasonably mimic synaptic conditions. The mean deactivation time constant τ was decreased for the H55E (54.22 ± 8.24 ms, n = 5, WT 85.65 ± 5.13 ms, n = 12 n = 12, p = 0.049) substitution, while the lysine mutation led to an increase in this time constant; but this change was not statistically significant. Finally, the alanine substitution (H55A 120.2 ± 8.77 ms, n = 9, p = 0.002) resulted in a significant slowdown of the deactivation time constant (Figure 3H, Figure 3I).

https://dx.doi.org/10.1021/acschemneuro.0c00781
ACS Chem. Neurosci. 2021, 12, 562−572

Model Simulations for Macroscopic Currents. To provide a mechanistic interpretation of the mutation effects, we performed trend model simulations for each mutation separately. For this purpose, a simplified scheme was used with one open and one desensitized state (Figure 4A).[19,33] Since the rise time was prolonged, the rapid macroscopic desensitization time constant was slowed down and deactivation-accelerated, and, most interestingly, for substitution with a positively charged amino acid (H55K), the opposite effects were observed except for deactivation mediated by the H55K mutant for which the change did not reach significance. The values of the rate constants for the WT receptors are given in the table shown in Figure 4. In our previous study,[33] we have reported that down-regulation of flipping/preactivation resulted in a slowdown of the onset and macroscopic desensitization of currents evoked by saturating [GABA]. Thus, the first step in an attempt to model the impact of the H55E mutation was to indicate proper δ and γ rate constants in a regime that the δ/γ ratio is lower than that for the WT receptors. Manipulations of δ (decrease) and γ (increase) allowed for reproduction of the increase in RT, but the increase in DES τ fast was too small to reproduce experimental observations indicating that besides flipping other rate constants need to be additionally altered. At the same time, deactivation τ was clearly shortened (to ca. 24 ms) reproducing qualitatively our experimental observations. When additionally reducing the desensitization rate d, a good qualitative agreement with all experimental observations was obtained (Figure 4A–4D). In the case of the H55K mutation, a reversal of changes in δ, γ, and d rate constants applied for H55E with additional down regulation of the r constant was considered, and our observations of shortened RT and accelerated desensitization were properly reproduced (Figure 4B–4C). In the case of the H55A mutation, for which we observed accelerated RT and desensitization with slower deactivation, an increase in δ, γ, and d was sufficient to qualitatively reproduce all our experimental observations (Figure 4A–4C). Importantly, these simulations predicted also that the extent of desensitization was reduced and increased in H55E and H55K (and H55A) mutations, respectively (in simulations, the extent of desensitization was calculated as a steady-state to peak ratio which can be compared to the experimentally determined FR10 value, Figure 2E). Taken altogether, the major conclusion from these minimum requirement macroscopic simulations is that the H55K and H55E mutations produce a mutually inverse effect on flipping/preactivation and desensitization, while the impact of the H55A mutation is grossly similar to that of H55K.

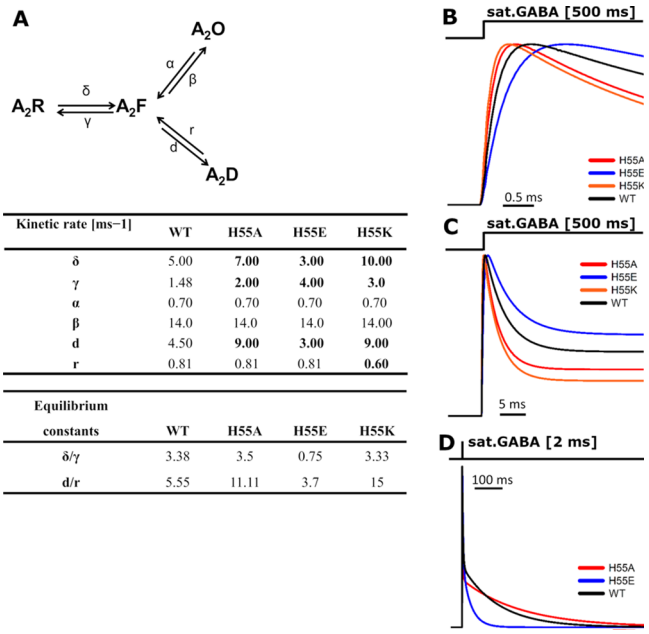

Kinetic rate [ms−1]	WT	H55A	H55E	H55K
δ	5.00	**7.00**	**3.00**	**10.00**
γ	1.48	**2.00**	**4.00**	**3.0**
α	0.70	0.70	0.70	0.70
β	14.0	14.0	14.0	14.00
d	4.50	**9.00**	**3.00**	**9.00**
r	0.81	0.81	0.81	**0.60**

Equilibrium constants	WT	H55A	H55E	H55K
δ/γ	3.38	3.5	0.75	3.33
d/r	5.55	11.11	3.7	15

Figure 4. Model simulations for macroscopic currents reveal changes in receptor gating due to mutations of H55 residues. (A) Kinetic model based on the so-called flipped Jones Westbrook model (see Results). Since experiments were performed in saturating conditions, the binding steps were omitted. The table presents rate constants for which an optimal reproduction of experimentally observed current time courses was obtained. Additionally, the equilibrium constants for flipping and desensitization are presented. Note that the largest alterations are predicted for flipping and desensitization (rates specified with bold). (B–D) Simulated responses for the onset, rapid desensitization, and deactivation, respectively, for WT (black), H55A (red), H55K (orange), and H55E (blue). The insets above the current traces indicate GABA applications.

impact of mutations on the dose–response relationships was minor, indicating a small effect on binding step, our simulations were carried out under the assumption that binding and unbinding rates are not affected. The macroscopic desensitization in our recordings was at least biphasic (Figure 3F); but the slow component(s) were clearly more distinct (much slower) than the rapid one, and the modeling was restricted to the time window of 30 ms within which the fast desensitization was predominant. The general strategy was to reproduce alterations in kinetics of current responses resulting from mutations by making minimum variations in the respective rate constants. The major features of currents that were considered in our modeling were the effects of H55 mutations on the following: current onset (Figure 3A), macroscopic desensitization (rate represented by DES τ fast and extent that can be deduced from FR10, Figure 3C), and deactivation after a short (2 ms) pulse (Figure 3H). Considering that the time constants of the rapid desensitization were in the range of ca. 2–7 ms, the FR10 value was close to the steady-state/peak (ss/peak) determined as a constant coefficient in the single-exponential fit for the rapid component (see Materials and Methods, eq 6). For H55E substitution, the

Single-Channel Recordings. To provide further insight into the impact of the H55 mutation on $GABA_AR$ gating, single-channel recordings were carried out in the cell-attached configuration at 10 mM GABA (Materials and Methods). In the case of all mutants (and WT receptors), there was a clear cluster activity (Figure 5A). As described in previous studies[36] and also by our group,[18,19] model activity was observed for considered mutants, and the predominant modes were identified as described in Materials and Methods. Namely, cluster P_{open} preanalysis (with Clampfit) revealed that the dominant modes for H55E, H55A, and H55K were characterized by P_{open} of approximately 0.75, 0.8, and 0.9, respectively (Figure 5B). Clusters identified in this way were then scanned using the SCAN software (DCProgs). A close inspection of single-channel activity and the post hoc distribution analysis with EKDIST (DCProgs) indicated that the resolution of 90 μs was optimal, allowing for reliably detecting the major kinetic components of events without any significant contribution of falsely marked short closures

https://dx.doi.org/10.1021/acschemneuro.0c00781
ACS Chem. Neurosci. 2021, 12, 562–572

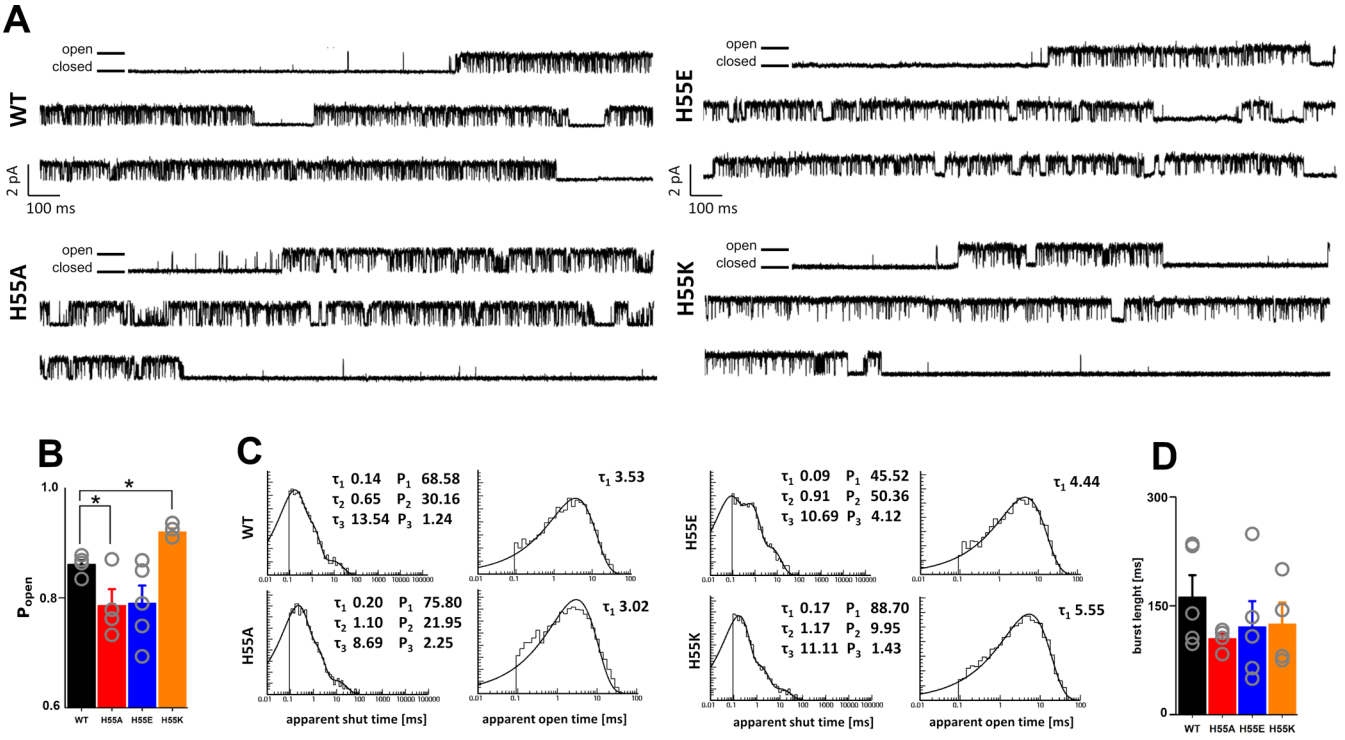

Figure 5. Single-channel analysis reveals that H55 mutations affect distributions of shut and open times. (A) Examples of single-channel traces for WT and each of the considered mutants. The most apparent difference is that in H55K openings are longer as they are more sparsely interrupted by short closures compared to WT and H55A. In H55E, closures appear to be less frequent than in WT, and their duration is slightly longer. The distribution parameters are given in Table 1. (B) Analysis of P_{open}. (C) Typical distributions for shut and open times. (D) Burst duration analysis reveals no significant changes between mutants and WT.

Table 1. Experimental and Simulated (0 μs res, Brackets) Values of Distributions Parameters for Shut and Open Times for H55 Mutants and WT[a]

	P_1	τ_1 [ms]	P_2	τ_2 [ms]	P_3	τ_3 [ms]	T_{shut} [ms]	T_{open} [ms]
WT	66.27 ± 3.36	0.13 ± 0.02	30.74 ± 3.11	0.62 ± 0.06	2.96 ± 1.23	10.73 ± 2.77	0.47 ± 0.06	3.44 ± 0.17
0 μs	[67.42 ± 4.10]	[0.13 ± 0.01]	[30.21 ± 4.09]	[0.58 ± 0.04]	[2.37 ± 0.54]	[13.97 ± 3.11]	[0.57 ± 0.08]	[2.17 ± 0.09]
H55A	75.80 ± 1.72	0.20 ± 0.02*	21.95 ± 1.84	1.10 ± 0.1*	2.25 ± 0.22	8.69 ± 0.63	0.59 ± 0.05	3.02 ± 0.49
0 μs	[73.56 ± 0.99]	[0.18 ± 0.01]*	[22.73 ± 1.33]*	[0.90 ± 0.05]*	[3.72 ± 0.49]	[9.23 ± 0.53]	[0.68 ± 0.05]	[2.05 ± 0.29]
H55E	45.52 ± 1.77*	0.09 ± 0.01	50.36 ± 1.37*	0.91 ± 0.11*	4.12 ± 1.29	10.21 ± 2.23	0.84 ± 0.1*	4.44 ± 0.21*
0 μs	[46.84 ± 2.01]*	[0.08 ± 0.01]*	[47.94 ± 1.25]*	[0.84 ± 0.10]*	[5.22 ± 1.40]	[10.70 ± 2.27]	[0.91 ± 0.11]*	[2.74 ± 0.1]*
H55K	88.70 ± 2.95*	0.17 ± 0.004	9.95 ± 2.59*	1.17 ± 0.12*	1.43 ± 0.41	11.11 ± 3.25	0.41 ± 0.06	5.55 ± 0.51*
0 μs	[84.49 ± 4.70]*	[0.15 ± 0.005]	[11.54 ± 3.58]*	[0.92 ± 0.09]*	[3.98 ± 1.22]	[15.10 ± 7.00]	[0.83 ± 0.25]	[3.41 ± 0.37]*

[a]Each mean value was obtained from at least four cells. Statistical significance with respect to WT is marked with bold and an "*".

affecting longer openings. In particular, in the case of mutants (especially H55E), when trying to analyze single-channel activity at higher resolution (e.g., 50−80 μs), excessive cell-to-cell variability especially of the fastest shut components was observed which made the statistics inconclusive. We thus decided to standardize the resolution at 90 μs. However, at this resolution, open time distributions could be fairly well described with only one component, while in our previous studies, at which higher resolution was applied, typically two components were reported.[18,19] Consequently, modeling of single-channel data was carried out using a simplified model with only one open state. In the above-described conditions, distributions of shut events, for each mutation and WT, were fitted with three exponential functions, and opening distributions, as already mentioned, were fitted with one exponential function (Figure 5C). The burst lengths were analyzed as described in Materials and Methods, and no significant differences were observed between mutants and the WT receptors (Figure 5D). As presented in detail in Table 1, considered mutations markedly affected the shut time distributions with respect to the WT receptors. In particular, a significant increase in the value of the first component (τ_1) was seen for H55A (0.2 ± 0.02 ms, n = 4, WT: 0.13 ± 0.02 ms, n = 7, p = 0.01). A similar trend was observed for H55K, and an opposite trend was observed for H55E; but these changes were not significant. The percentage P_1 for H55E significantly decreased (45.52 ± 1.77 vs 68.58 ± 4.34, p = 0.001), whereas for H55K it increased (88.7 ± 2.95, n = 4, p = 0.016). For H55A, a trend toward an increase was apparent, but it was not significant. The second shut time component (τ_2) was significantly increased for H55K (1.17 ± 0.12 ms, n = 4, WT: 0.65 ± 0.05 ms, n = 5, p = 0.003), for H55A (1.1 ± 0.1 ms, n = 4; p = 0.003), and also (surprisingly) for H55E (0.9 ± 0.1, n = 5, p = 0.03). The percentage P_2 for this component was significantly altered for H55E (50.36 ± 1.37, n = 5, WT: 30.16 ± 4.31, n = 5, p = 0.008) and H55K (9.95 ± 2.59, n = 4,

https://dx.doi.org/10.1021/acschemneuro.0c00781
ACS Chem. Neurosci. 2021, 12, 562−572

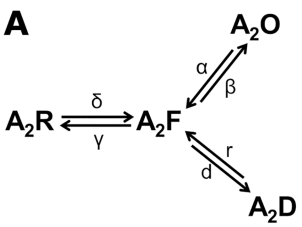

Kinetic rate constants [ms^{-1}]	WT	H55A	H55E	H55K
δ	2.54 ± 0.34	**↓1.39 ± 0.09***	2.34 ± 0.3	**↓1.11 ± 0.12***
γ	1.42 ± 0.29	0.79 ± 0.09	**↑4.99 ± 0.39***	**↓0.44 ± 0.11***
α	0.52 ± 0.04	0.52 ± 0.07	**↓0.35 ± 0.005***	**↓0.3 ± 0.03***
β	5.73 ± 0.25	**↓4.32 ± 0.31***	6.85 ± 0.62	5.54 ± 0.2
d	0.24 ± 0.07	0.15 ± 0.03	0.33 ± 0.09	0.15 ± 0.04
r	0.16 ± 0.05	0.11 ± 0.006	0.12 ± 0.03	0.11 ± 0.04
Equilibrium rate	**WT**	**H55A**	**H55E**	**H55K**
δ/γ	1.65 ± 0.25	1.80 ± 0.12	**↓0.48 ± 0.07***	**↑2.89 ± 0.45***
β/α	13.09 ± 1.31	9.05 ± 1.89	**↑18.68 ± 1.68***	**↑18.83 ± 1.32***
d/r	1.67 ± 0.29	1.37 ± 0.23	2.73 ± 0.36	2.73 ± 1.46

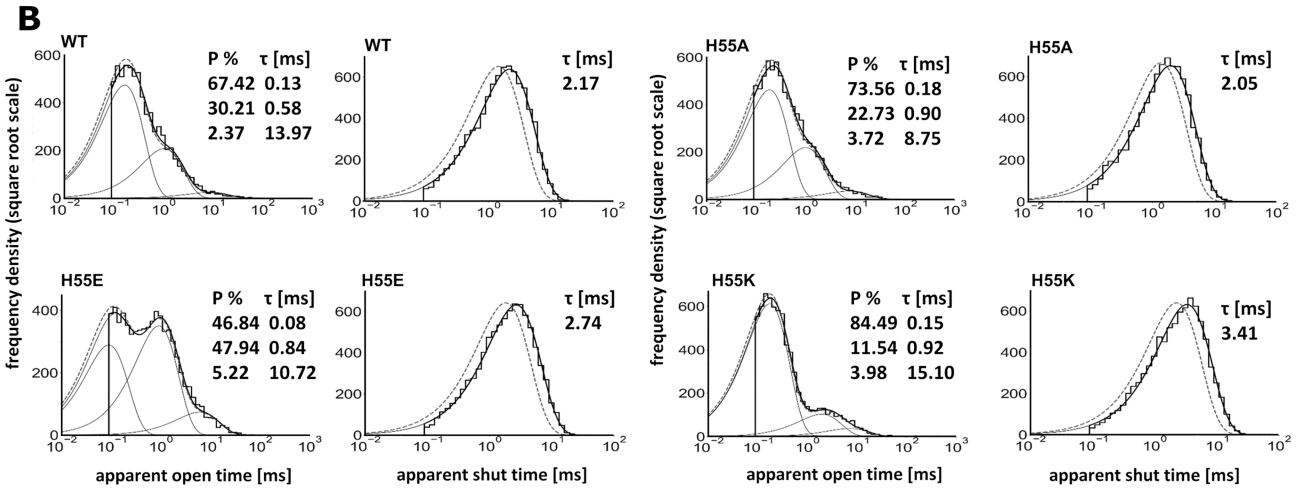

Figure 6. Model simulations of single-channel data indicate the impact of the H55 mutation on the receptor gating. (A) Flipped Jones and Westbrook's model with binding steps omitted because of agonist saturation. The table presents the values of kinetic rate constants (statistical significance with respect to WT are marked with bold and an "*"). Each mean value was obtained from at least four cells. (B) Examples of simulated shut and open times distributions with respective time constants (τ) and percentages (P). Distributions determined for 0 μs time resolution (correction for missed events) are drawn with gray dashed lines. All distribution parameters are presented in Table 1.

p = 0.016), and again, these changes occurred in the opposite directions with respect to WT receptors. None of the considered mutations affected the third shut time component τ_3 or its percentage P_3 (Table 1). Based on these distribution parameters, the mean closed times were calculated, and only for H55E an increase to 0.84 ± 01 ms from 0.45 ± 0.05 ms (for WT, p = 0.008) was observed (Table 1). The open time distribution was mostly affected in the case of H55K in which the value of the open time constant was significantly larger compared to WT (H55K: 5.55 ± 0.51 ms, n = 4, WT: 3.53 ± 0.18 ms, n = 5, p = 0.005). A significant increase was also observed for H55E (4.44 ± 0.21 ms, n = 5, p = 0.011), and H55A did not affect the open times distribution. Notably, in the case of open times distributions, both H55E and H55K induced open times alterations in the same direction, in contrast to closed times and parameters describing macroscopic currents (Figure 3).

In addition, in Table 1, we provide the values of parameters for 0 μs resolution (with correction for missed events) obtained with HJCFIT software (DCProgs).

Single-Channel Modeling. For the kinetic description of the H55 residue substitution impact, we chose the same model framework (Figure 6A) as we did for macroscopic modeling. Since GABA concentration was saturating and the agonist was continuously present during the entire recording period (stationary conditions), the binding steps described by k_{on} and k_{off} rates were omitted. To optimize the values of the rate constants, the HJCFIT (DCProgs) software was used. Each cell was represented by respective .SCN files (input to the HJCFIT) for which a set of the rate constants was obtained. The statistics of so obtained rate constants for WT receptors and considered mutants is summarized in the table shown in Figure 6. Interestingly, both in the case of H55K and H55A, the flipping rates δ were significantly decreased (H55K: p = 0.002, n = 4, H55A: n = 4, p = 0.0001, WT: n = 7), and for H55E, the change of this rate did not reach statistical significance. The unflipping rate γ was significantly increased (n = 5, p = 0.001) for H55E and decreased for H55K (n = 4, p = 0.03) and for H55A, but for the latter, change was not significant. Notably, the flipping/preactivation equilibrium constant (δ/γ) showed a prominent and significant (n = 5, p = 0.004; n = 4, p = 0.03) decrease and increase for H55E and H55K, respectively, whereas for H55A, its value was close to that in WT receptors (table shown in Figure 6). Thus, these simulations demonstrate that the mutation at the H55 residue affects the flipping/preactivation transition, and different charges of the substituting residues gave rise to opposite changes in the flipping equilibrium constants. Our analysis revealed that besides alterations in flipping/preactivation, the considered mutations affect also the opening/closing transitions. The closing rate α is significantly decreased both for H55E and H55K (H55E: n = 5, p = 0.002, H55K: n = 4, p =

https://dx.doi.org/10.1021/acschemneuro.0c00781
ACS Chem. Neurosci. 2021, 12, 562−572

0.002), thus surprisingly, the changes go in the same directions. The opening rate β is significantly reduced only for H55A (n = 4, p = 0.014). Interestingly, the equilibrium constant for opening/closing transitions (β/α) significantly increased for both H55E and H55K, while for H55A, no significant change was found. Desensitization (d) and resensitization (r) rates were found not to be affected by considering mutations, but it needs to be considered that in the stationary conditions the estimation of these transitions is limited (see Discussion). Taken altogether, these simulations of the single-channel activity based on detected events (*.SCN files) provide further evidence that the considered mutations affect flipping/preactivation and indicate also a relatively minor effect on opening/closing transitions.

Substitution of the H55 Residue Alters $GABA_AR$ Gating. The major finding of the present work is that the mutation of H55 at the ECD−TMD interface of the α_1 subunit markedly affects various stages of receptor gating, primarily flipping/preactivation and desensitization and also, to some extent, opening/closing. In a previous study, Kash and co-workers[29] investigated the impact of the H56 mutation (human α_1 subunit, in our case from rat) and found that the mutation with lysine caused a leftward shift of the dose−response which differs from our observations (no effect, Figure 2). Notably, the H55K mutant was characterized by a particularly rapid kinetics with pronounced macroscopic desensitization (faster and more profound than in WT, Figure 3). Such a short lasting spike-like current component could go largely undetected with a relatively slow perfusion (approximately 50 ms)[29] which could result in distortion of the dose−response. However, similar to our observations (Figure 1), they observed a slight rightward dose−response shift for the H55E mutant. This similarity may result from the fact that this mutation resulted in a slowdown of the receptor kinetics making its characterization more reliable with a slower perfusion system. Although the considered mutations of the H55 residue are not fully detrimental for the receptor function, the extent of its kinetic alteration would be likely to produce a substantial effect on synaptic integration which occurs at a millisecond or even submillisecond time scale. In this context, the alteration of deactivation by nearly 50% (in either direction) appears to be particularly important as this process is believed to reflect the duration of GABAergic synaptic currents. Indeed, the agonist presence within the synaptic cleft during transmission at a GABAergic synapse is short lasting, up to 1 ms,[37−39] and therefore, time duration of IPSC reflects primarily the timing of the deactivation process. Thus, alteration of deactivation kinetics would be expected to proportionally affect the charge transfer (integral of synaptic current) during synaptic transmission. The impact of mutations on the current rise time appears minor (less than 1 ms), but it needs to be considered that AMPA receptor mediated excitatory synaptic currents could operate at a submillisecond time scale, and therefore, such an apparently minor alteration of the GABAergic current onset might still affect the synaptic integration.

Notably, our conclusions regarding gating modifications derived from macroscopic and single-channel analysis were not exactly overlapping. In particular, single-channel analysis and modeling revealed only minor and nonsignificant changes in desensitization rate constants (table shown in Figure 6), whereas macroscopic investigations strongly underscored the impact of the H55 mutation on these transitions. A similar discrepancy was observed in our previous papers,[18,20] and it was attributed primarily to profoundly different experimental conditions: nonequilibrium (macroscopic) vs steady-state (single-channel). Indeed, whereas in rapid application experiments, the vast majority of receptors desensitizes within a few milliseconds, in the single-channel recordings, the rapid desensitization may have a contribution to some components of shut times distributions, while longer sojourns in the desensitized states are not included in the clusters. The largest changes due to H55 mutations were observed in the flipping/preactivation rate constants (σ and γ). Although for the flipping equilibrium constant (σ/γ), macroscopic and single-channel modeling led to qualitatively analogous predictions, some discrepancies appeared at the level of specific rate constants. In macroscopic simulations, the flipping/preactivation rate σ for H55E and H55K had to be decreased and increased, respectively, while in single-channel modeling, a significant change (decrease) in σ was predicted only for H55K. A qualitative agreement at the level of the equilibrium constants was obtained because in the single-channel modeling γ strongly increased for H55E and decreased for H55K. The reasons for which differences in estimations of σ and γ in macroscopic and single-channel analysis were observed are not clear. We may speculate that in the case of these mutants, in highly dynamic conditions, the receptor might operate in a different mode than in the steady-state. However, when we analyzed other mutants such as α_1F64,[18,33] β_2E155,[21] or α_1F45,[20] there was typically a good qualitative correspondence between gating parameters (except for desensitization) estimated from macroscopic and single-channel activity. We may speculate that in these different situations, the mutation at this critical interface domain might differentiate the *modus operandi* of this receptor in steady-state and dynamic conditions.

It is worth mentioning that standardization of resolution at 90 μs in the single-channel analysis presented here resulted in slight differences in estimation of the rate constants with respect to the previous reports in which analysis was carried out at higher resolution.[18,19] These differences, however, are unlikely to affect our conclusions based on single-channel recordings.

Impact of Charged Residues at H55. Interestingly, desensitization transitions (described based on macroscopic recordings) showed a similar dependence on the electric charge of amino acid substituting H55 as in the case of preactivation/flipping−enhancement for K and attenuation for E. This might suggest an overall tendency for $GABA_AR$ gating to depend on local electrostatic interactions in the vicinity of H55. However, to our surprise, the changes in the opening/closing (β/α) went in the same direction for the two mutants. This may indicate differences in molecular mechanisms underlying flipping and opening/closing. However, analysis of macroscopic currents did not provide any obvious indication for a change in opening/closing transitions, suggesting that such an effect might take place preferentially in the stationary conditions. Considering that the changes in β/α observed for H55K and H55E mutants were considerably smaller with respect to those determined for σ/γ and were not apparent in macroscopic analysis, we tend to consider this effect as minor, and the primary impact of H55 on receptor gating we ascribe to preactivation/flipping and desensitization.

The major question that arises from the data presented in this report concerns the molecular scenarios whereby

https://dx.doi.org/10.1021/acschemneuro.0c00781
ACS Chem. Neurosci. 2021, 12, 562−572

considered mutations affect the receptor gating. The observed strong impact of electrical charges is not surprising as H55 is not electrostatically neutral and is surrounded by negatively charged residues (D54, D56, Figure 1). Moreover, considering that pK_a for histidine is relatively close to physiological pH, it cannot be excluded that H55 might switch between deprotonated and protonated forms in response to local variations at the pH level which could occur, e.g., due to release of acidic content of synaptic vesicles.[40] It is thus possible that H55 influences electrostatic interaction between the $\beta1-\beta2$ and M2−M3 loops which was known to play a critical role in receptor activation.[28] The influence of H55 on local electrostatic interactions needs not to be limited to the nearest salt bridges and closest neighbors. In agreement with the concept suggested by Xiu and co-workers[41] that "overall charging pattern of the gating interface" rather than specific pairwise interactions controls gating, it seems likely that H55/Loop2 (Figure 1) participates in shaping of the local electrostatic landscape affecting receptor functioning. Involvement of local electrostatic interaction at the $GABA_A$ receptor interface region in receptor gating was also found in other locations.[28,30,42] Considering a key role of the interface electrostatics, we may speculate that an increase in opening/closing constants β/α for H55K and H55E substitutions might reflect a stabilizing role of electric charge on the open conformation of the receptor. Such a role for electrostatics on protein stability has been proposed for other systems.[43,44] Such a hypothetic mechanism would corroborate our observation that H55 substitution with a small and neutral amino acid, alanine, did not affect opening/closing.

H55 Affects Gating via Long-Range Interactions. An intriguing issue is the molecular mechanism underlying a marked impact of the H55 mutation on the desensitization process. A strong involvement of the ECD−TMD interface in regulating these transitions reported here seems to be supported by an observation by Wang and Lynch[27] who used voltage clamp fluorometry and implicated involvement of this region in the desensitization of glycine receptors. However, in a more recent work,[45] Gielen and co-workers proposed that desensitization of $GABA_AR$ is regulated by interactions between the second and third transmembrane segment. It is possible that interaction between the $\beta1-\beta2$ (which contains H55) and the M2−M3 loops may provide the mechanism whereby H55 might influence the desensitization gate indicated by Gielen and co-workers. Although involvement of transmembrane segments in regulating desensitization is well substantiated,[45] our previous studies indicated that other portions of $GABA_AR$ macromolecules might be also involved in mechanisms underlying desensitization. In our recent work,[46] we reported that flurazepam affected desensitization. Considering that the benzodiazepine binding site is located at the ECD, very distantly from transmembrane segments indicated by Gielen and co-workers,[45] it seems likely that desensitization might be additionally controlled by some structures at the ECD. Moreover, in our recent study,[20] we reported that desensitization is strongly affected by the mutation of the F45 residue, located at the loop G of the α_1 subunit, close to the agonist binding site. Even more surprisingly, in our most recent paper,[47] we report that the mutation of α_1F14 and β_2F31 residues, located at the "top" of the ECD, also influences the desensitization transitions. Thus, from our studies, a picture emerges that desensitization might be controlled by vast fragments of $GABA_AR$ macromolecules indicating a concept of a "diffuse" desensitization gate rather than its strict and well-defined localization. This view is compatible with the aforementioned proposal that $GABA_AR$ functioning is determined by long-range interactions leading to its cooperative mode of action. Interestingly, in the GLIC channel, desensitization was found to be associated with movements of transmembrane segments which resulted from a wide range of rearrangements of interfacial loops and related intersubunit interactions[48] pointing to a widespread structural mechanism of this conformational transition. Such a "global view" on conformational transitions is further supported by studies demonstrating a strong lateral intersubunit interaction in $GABA_AR$.[30] In addition, for related pentameric channels GLIC and ELIC, a concerted counterclockwise movement comprising both the ECD and TMD was implicated further underscoring the importance of long-range interactions resulting in quaternary twist and tertiary deformation.[49]

Taken altogether, this study identifies the role of the H55 residue at the α_1 subunit in specific gating transitions, primarily flipping/preactivation and desensitization, and sheds new light on the electrostatic nature of its involvement in $GABA_AR$ functioning. A further understanding of molecular mechanisms underlying the conformational transitions of $GABA_ARs$ is necessary to open new avenues in understanding the physiology of GABAergic inhibition and in designing clinically relevant modulators of these receptors.

MATERIALS AND METHODS

Cell Cultures. All of the experiments (macroscopic and single-channel recordings) were performed using the human embryonic kidney 293 (HEK293) cell line (European Collection of Authenticated Cell Culture). The cells were cultured in Gibco DMEM with Glutamax supplemented with 10% FBS and 1% penicillin/streptomycin (all from Thermo Fisher Scientific) in a humidified atmosphere with 5% CO_2 at 37 °C. For experiments, cells were replated on poly-D-lysine (1 μg/mL, Sigma) coated 12 mm ø glass coverslips. Cells were grown for at least 48 h and then were transfected with FuGene HD (Promega, US) 24 h before the experiment. cDNA plasmids used for cells transfection were based on a cytomegalovirus promoter (pCMV) and contained the coding sequence for rat (*Rattus norvegicus*) $GABA_A$ receptor α_1, β_2, and γ_{2L} subunits and eGFP to help identify transfected cells. The amount of cDNA used for transfection was, respectively, 0.5:0.5:1.5:0.5 μg (α_1:β_2:γ_{2L}:eGFP), which was optimal to ensure sufficient expression to carry out the electrophysiological experiments. Moreover, judging from the amplitudes of recorded currents, substitution of the 55th residue at the α_1 subunit did not have any major effect on the receptor expression. Successfully transfected cells were visualized with a fluorescence illuminator (470 nm wavelength, CoolLED, UK). All electrophysiological experiments were carried out with a modular inverted microscope (Leica DMi8, Germany).

Electrophysiological Recordings. Macroscopic current recordings were performed using the patch clamp technique in the outside-out excised-patch configuration, 24 h after transfection at a holding potential of −40 mV, and signals were filtered with an 8-pole low-pass Bessel filter set at 10 kHz using an Axopatch 200B (Molecular Devices, US) amplifier. The signal was then digitized with a Digidata 1550A card (Molecular Devices, US). Acquisition of signals was performed with pClamp 10.7 software (Molecular Devices, US). Pipettes used in experiments were pulled from borosilicate glass (outer ø, 1.5 mm; inner ø, 1.05 mm; Science Products) using a P-97 horizontal puller (Sutter Instruments, US) to achieve final resistance in the range 2.5−3.5 MΩ when filled with an intracellular solution that contained (in mM) 137 KCl, 1 $CaCl_2$, 2 ATP-Mg, 2 $MgCl_2$, 10 K-gluconate, 11 EGTA, and 10 HEPES, with the pH adjusted to 7.2 with KOH. An external solution consisted of (in mM) the following: 137 NaCl, 5 KCl, 2 $CaCl_2$, 1 $MgCl_2$, 10 HEPES, and 20 D-(+)-glucose

https://dx.doi.org/10.1021/acschemneuro.0c00781
ACS Chem. Neurosci. 2021, 12, 562−572

(pH adjusted to 7.2 with NaOH). For experiments with high GABA concentrations (>10 mM), a low-chloride solution was used to keep osmolarity at ∼330 mOsm: intrapipette (in mM): 87 KCl, 1 $CaCl_2$, 2 $MgCl_2$, 50 K-gluconate, 11 EGTA, 10 HEPES, and 2 ATP-Mg (pH adjusted to 7.2 with KOH) and external (in mM): 87 NaCl, 5 KCl, 2 $CaCl_2$, 1 $MgCl_2$, 10 HEPES, and 20 D-(+)-glucose (pH adjusted to 7.2 with NaOH, with final osmolality adjusted with glucose as described earlier by ref 33). Solutions with high [GABA] (>10 mM) were used upon construction of dose−response relationships to ascertain that saturation was achieved. Rapid application of a GABA-containing solution was effectuated using the theta glass tube mounted on a piezoelectric-driven translator (Physik Instrumente, Germany) as described in detail by refs 33, 50, and 51. Solutions were supplied into the two channels of the theta glass tube by a high-precision SP220IZ syringe pump (World Precision Instruments, US). The open tip exchange time achieved using this technique was within 70−120 μs. The time course of the macroscopic desensitization was described by fitting with a single exponential function (implemented in Clampfit, MolecularDevices, US) as

$$I(t) = Ae^{\frac{-t}{\tau}} + C \tag{1}$$

The current deactivation time course after a 2-ms application of the saturating GABA pulse was fitted with a biexponential function:

$$I(t) = A_1 e^{\frac{-t}{\tau_1}} + A_2 e^{\frac{-t}{\tau_2}/} \tag{2}$$

The deactivation time constant was calculated as

$$\tau = \%A_1\tau_1 + \%A_2\tau_2 \tag{3}$$

where

$$\%A_1 = \frac{A_1}{A_1 + A_2} \text{ and } \%A_2 = \frac{A_2}{A_1 + A_2} \tag{4}$$

Rise time was (RT) calculated as 10%−90% of the macroscopic current onset. Dose−response relationships were described with standard Hill's equation in the form

$$\mathrm{EC} = \frac{1}{1 + \left(\frac{\mathrm{EC}_{50}}{[\mathrm{GABA}]}\right)^{n_h}} \tag{5}$$

where [GABA] is the agonist concentration, and n_h is the Hill's coefficient.

Kinetic modeling of macroscopic currents was performed with Channel Lab software (Synaptsof Inc. US). The model used for macroscopic current simulation (Figure 4) was based on the flipped Jones-Westbrook model used previously.[33] In our modeling, we have considered only one, rapidly desensitizing state which, upon application of saturating [GABA], reached steady-state within 2−10 ms, and we limited the analysis of this process to this time window. Thus, the values of the FR10 parameter were close to the steady-state to peak ratio determined as a constant coefficient in the single exponential fit (eq 1).

$$\mathrm{ss/peak} = \frac{C}{A} \tag{6}$$

Single-channel recordings were performed in the cell-attached configuration of the patch clamp technique 24 h after transfection at a holding pipet potential of 100 mV and an 8-pole low-pass Bessel filter set at 100 kHz using an Axopatch 200B (Molecular Devices, US) amplifier. The signal was digitized with a Digidata 1550B card (Molecular Devices, US) with the hum silencer option on. The acquisition of a signal was performed with pClamp 10.7 software (Molecular Devices, US). Pipettes used in experiments were pulled from borosilicate glass (outer ø, 1.5 mm; inner ø, 0.86 mm; Science Products, Germany) using a P-1000 horizontal puller (Sutter Instruments, US). To reduce noise, pipettes were coated with Sylgard (Dow Corning, US) and heat-polished to achieve final resistance in the range of 10−15 MΩ. An extracellular (and intrapipette) solution consisted of (in mM) 102.7 NaCl, 20 Na-gluconate, 2 KCl, 2 $CaCl_2$, 1.2 $MgCl_2$, 10 HEPES (Carl Roth, Germany), 20 TEA-Cl, 14 D-(+)-glucose, and 15 sucrose (Carl Roth, Germany), dissolved in deionized water with the pH adjusted to 7.4 with 2 M NaOH. To keep noise as low as possible, the level of the extracellular solution was kept at a minimal possible level. Recorded traces were selected for further analysis if the patches had stable seal resistance of at least 10 GΩ. Single-channel analysis used here is described in detail in ref 18. Briefly, all of the electrophysiological recordings were conducted at room temperature (20−23 °C). Recordings were stored in .abf format and filtered to achieve a signal-to-noise ratio of at least 15. The final cut off frequency (f_c) was calculated as

$$\frac{1}{f_c} = \frac{1}{f_a} + \frac{1}{f_d} \tag{7}$$

where f_a is the frequency value for the analogue filter, and f_d is the frequency for digital filtering performed with an 8-pole low-pass Bessel filter effectuated with Clampfit software (Molecular Devices, US). Single-channel recordings for H55 mutants revealed cluster activity with apparently different activity modes−the feature already observed by Lema and Auerbach[36] and by our group.[18,19] However, in the present case, modes showed relatively small differences, and their precise distinction by eye was problematic. To select the dominant activity mode for each mutation, clusters were prescanned with Clampfit (Molecular Devices, US) to determine the P_{open} values for each of them. Then clusters with dominant modes of activity were idealized with SCAN software (DCProgs, http://www.onemol.org.uk/ kindly provided to us by David Colquhoun) and stored as .SCN files. For further analysis, only traces containing ∼10000 events (understood as a number of closures and openings summed up) were considered. Typically, a few clusters were sufficient to accomplish this number of events. In the next step, .SCN files were used to create shut and open time distributions with EKDIST software (DCProgs). To determine the rate constants describing the single-channel kinetics, the .SCN files were analyzed with HJCFIT software (DCProgs) by applying the maximum likelihood method for the predefined kinetic scheme. Since the conditions of saturating [GABA] were considered, in the models, the binding steps were omitted.[18,19] Burst length was determined by so-called critical time (tcrit) whose determination was based on analysis of shut time distribution obtained with EKDIST software (DCProgs). Tcrit was obtained using Jackson criterion[52] applied to the second and the third shut time components. In the statistics, "n" refers to the number of patches which were always done on new cells.

Unless otherwise stated, all of the chemicals used in the above experiments were purchased from Sigma-Aldrich, Merck.

Statistical Analysis. Comparisons between groups were performed using the unpaired Student's t-test preceded by the Grubbs' test for outlier values, and tests for normality and equality of variance were performed using Shapiro-Wilk's and Levene's tests, respectively. In the case of data sets for which the normality test failed, the U-Mann−Whitney test was used. All comparisons with the t-test were performed only for control and tested groups; no multiple comparisons were performed. The difference between the two compared groups was considered significant if $p < 0.05$. Statistical analyses were performed using SigmaPlot 11.0 (Systat Software, US), Excel 2016 (Microsoft, US.).

All the data are presented as mean ± SEM value. In the case of data obtained from macroscopic recordings, for graphical visualization in the form of bar plots, all mean values were standardized to those determined for WT as the control group. Data points collected for WT receptors ($WT_{data.point}$) were standardized ($WT_{std.data.point}$) as follows

$$WT_{std.data.point} = \frac{WT_{data.point}}{WTmean} \tag{8}$$

where WTmean is the mean for a respective parameter. Accordingly, for mutants, standardized mean value parameters ($H55_{std.mean}$) were calculated as

https://dx.doi.org/10.1021/acschemneuro.0c00781
ACS Chem. Neurosci. 2021, 12, 562−572

$$H55_{std.mean} = \frac{H55mean}{WTmean} \quad (9)$$

and single standardized data point ($H55_{data.std.point}$) for parameters collected for H55 mutants were calculated as

$$H55_{data.std.point} = \left(\frac{H55_{data.point}}{H55mean}\right) \times \left(\frac{H55mean}{WTmean}\right) \quad (10)$$

AUTHOR INFORMATION

Corresponding Authors

Przemyslaw T. Kaczor − *Department of Biophysics and Neuroscience, Wroclaw Medical University, Wroclaw, Dolnoślaskie 50-368, Poland*; orcid.org/0000-0003-1224-0098; Email: przemyslaw.kaczor@umed.wroc.pl

Jerzy W. Mozrzymas − *Department of Biophysics and Neuroscience, Wroclaw Medical University, Wroclaw, Dolnoślaskie 50-368, Poland*; Phone: +48 71 784 14 00; Email: jerzy.mozrzymas@umed.wroc.pl

Author

Aleksandra D. Wolska − *Department of Biophysics and Neuroscience, Wroclaw Medical University, Wroclaw, Dolnoślaskie 50-368, Poland*

Complete contact information is available at: https://pubs.acs.org/10.1021/acschemneuro.0c00781

Author Contributions

P.T.K. performed the experiments, data analysis, model simulations, structure visualization and alignment, and data visualization and wrote the first draft of the manuscript. A.D.W. performed part of the experiments and contributed to data analysis. J.W.M. conceived the project, provided financial support, supervised project realization, and participated in designing the experiments, data analysis, and model simulations, writing, and editing the final version of the manuscript.

Funding

This work was financed by Polish National Science Centre grant MAESTRO, number: DEC-2015/18/A/NZ1/00395.

Notes

The authors declare no competing financial interest.

ACKNOWLEDGMENTS

Special thanks go to Ilona Iżykowska from the Department of Biophysics and Neuroscience for plasmid preparations used in transfection and Michal A. Michalowski from the Department of Biophysics and Neuroscience for help in identifying amino acid residues considered in this work and for critical reading of the manuscript.

ABBREVIATIONS

ECD - extracellular domain
TMD - transmembrane domain
$GABA_AR$ - γ-aminobutyric acid receptor type A
[GABA] - γ-aminobutyric acid concentration
WT - wild type of γ-aminobutyric acid receptor type A
H55 - 55th residue of α_1 subunit of γ-aminobutyric acid receptor type A
H55A/E/K - substitution of the H55 residue of the α_1 subunit of γ-aminobutyric acid receptor type A with alanine, lysine, or glutamic acid
FR10/500 - percentage of the remaining current evoked by [GABA] application at 10/500 ms after peak amplitude

REFERENCES

(1) Thompson, A. J., Lester, H. A., and Lummis, S. C. (2010) The structural basis of function in Cys-loop receptors. *Q. Rev. Biophys. 43*, 449−499.
(2) Mody, I., and Pearce, R. A. (2004) Diversity of inhibitory neurotransmission through GABA(A) receptors. *Trends Neurosci. 27*, 569−575.
(3) Farrant, M., and Nusser, Z. (2005) Variations on an inhibitory theme: phasic and tonic activation of GABA(A) receptors. *Nat. Rev. Neurosci. 6*, 215−229.
(4) Hosie, A. M., Wilkins, M. E., da Silva, H. M. A., and Smart, T. G. (2006) Endogenous neurosteroids regulate GABAA receptors through two discrete transmembrane sites. *Nature 444*, 486−489.
(5) Christian, C. A., and Huguenard, J. R. (2013) Astrocytes potentiate GABAergic transmission in the thalamic reticular nucleus via endozepine signaling. *Proc. Natl. Acad. Sci. U. S. A. 110*, 20278−20283.
(6) Rudolph, U., and Knoflach, F. (2011) Beyond classical benzodiazepines: novel therapeutic potential of GABAA receptor subtypes. *Nat. Rev. Drug Discovery 10*, 685−697.
(7) Rudolph, U., and Möhler, H. (2004) Analysis of GABAA Receptor Function and Dissection of the Pharmacology of Benzodiazepines and General Anesthetics Through Mouse Genetics. *Annu. Rev. Pharmacol. Toxicol. 44*, 475−498.
(8) Feng, H.-J., and Forman, S. A. (2018) Comparison of αβδ and αβγ GABAA receptors: Allosteric modulation and identification of subunit arrangement by site-selective general anesthetics. *Pharmacol. Res. 133*, 289−300.
(9) Ernst, B. J., Clark, G. F., and Grundmann, O. (2015) The Physicochemical and Pharmacokinetic Relationships of Barbiturates - From the Past to the Future. *Curr. Pharm. Des. 21*, 3681−3691.
(10) Sieghart, W., and Savić, M. M. (2018) International Union of Basic and Clinical Pharmacology. CVI: GABAA Receptor Subtype- and Function-selective Ligands: Key Issues in Translation to Humans. *Pharmacol. Rev. 70*, 836.
(11) Masiulis, S., Desai, R., Uchanski, T., Serna Martin, I., Laverty, D., Karia, D., Malinauskas, T., Zivanov, J., Pardon, E., Kotecha, A., Steyaert, J., Miller, K. W., and Aricescu, A. R. (2019) GABAA receptor signalling mechanisms revealed by structural pharmacology. *Nature 565*, 454−459.
(12) Phulera, S., Zhu, H., Yu, J., Claxton, D. P., Yoder, N., Yoshioka, C., and Gouaux, E. (2018) Cryo-EM structure of the benzodiazepine-sensitive alpha1beta1gamma2S tri-heteromeric GABAA receptor in complex with GABA. *eLife 7*, e39383.
(13) Laverty, D., Desai, R., Uchanski, T., Masiulis, S., Stec, W. J., Malinauskas, T., Zivanov, J., Pardon, E., Steyaert, J., Miller, K. W., and Aricescu, A. R. (2019) Cryo-EM structure of the human alpha1beta3gamma2 GABAA receptor in a lipid bilayer. *Nature 565*, 516−520.
(14) Zhu, S., Noviello, C. M., Teng, J., Walsh, R. M., Kim, J. J., and Hibbs, R. E. (2018) Structure of a human synaptic GABAA receptor. *Nature 559*, 67−72.
(15) Miller, P. S., and Aricescu, A. R. (2014) Crystal structure of a human GABAA receptor. *Nature 512*, 270−275.
(16) Kim, J. J., Gharpure, A., Teng, J., Zhuang, Y., Howard, R. J., Zhu, S., Noviello, C. M., Walsh, R. M., Jr., Lindahl, E., and Hibbs, R. E. (2020) Shared structural mechanisms of general anaesthetics and benzodiazepines. *Nature 585*, 303−308.
(17) Miller, P. S., and Smart, T. G. (2010) Binding, activation and modulation of Cys-loop receptors. *Trends Pharmacol. Sci. 31*, 161−174.
(18) Kisiel, M., Jatczak, M., Brodzki, M., and Mozrzymas, J. W. (2018) Spontaneous activity, singly bound states and the impact of alpha1Phe64 mutation on GABAAR gating in the novel kinetic model based on the single-channel recordings. *Neuropharmacology 131*, 453−474.

(19) Terejko, K., Kaczor, P. T., Michalowski, M. A., Dabrowska, A., and Mozrzymas, J. W. (2020) The C loop at the orthosteric binding site is critically involved in GABAA receptor gating. *Neuropharmacology 166*, 107903.
(20) Brodzki, M., Michałowski, M. A., Gos, M., and Mozrzymas, J. W. (2020) Mutations of α1F45 residue of GABAA receptor loop G reveal its involvement in agonist binding and channel opening/closing transitions. *Biochem. Pharmacol. 177*, 113917.
(21) Jatczak-Śliwa, M., Kisiel, M., Czyzewska, M. M., Brodzki, M., and Mozrzymas, J. W. (2020) GABA(A) Receptor β(2)E155 Residue Located at the Agonist-Binding Site Is Involved in the Receptor Gating. *Front. Cell. Neurosci. 14*, 2.
(22) Newell, J. G., McDevitt, R. A., and Czajkowski, C. (2004) Mutation of glutamate 155 of the GABAA receptor beta2 subunit produces a spontaneously open channel: a trigger for channel activation. *J. Neurosci. 24*, 11226−11235.
(23) Laha, K. T., and Tran, P. N. (2013) Multiple tyrosine residues at the GABA binding pocket influence surface expression and mediate kinetics of the GABAA receptor. *J. Neurochem. 124*, 200−209.
(24) Connolly, C. N., and Wafford, K. A. (2004) The Cys-loop superfamily of ligand-gated ion channels: the impact of receptor structure on function. *Biochem. Soc. Trans. 32*, 529−534.
(25) Cederholm, J. M. E., Schofield, P. R., and Lewis, T. M. (2009) Gating mechanisms in Cys-loop receptors. *Eur. Biophys. J. 39*, 37.
(26) Bertozzi, C., Zimmermann, I., Engeler, S., Hilf, R. J. C., and Dutzler, R. (2016) Signal Transduction at the Domain Interface of Prokaryotic Pentameric Ligand-Gated Ion Channels. *PLoS Biol. 14*, e1002393−e1002393.
(27) Wang, Q., and Lynch, J. W. (2011) Activation and desensitization induce distinct conformational changes at the extracellular-transmembrane domain interface of the glycine receptor. *J. Biol. Chem. 286*, 38814−38824.
(28) Kash, T. L., Jenkins, A., Kelley, J. C., Trudell, J. R., and Harrison, N. L. (2003) Coupling of agonist binding to channel gating in the GABAA receptor. *Nature 421*, 272−275.
(29) Kash, T. L., Kim, T., Trudell, J. R., and Harrison, N. L. (2004) Evaluation of a proposed mechanism of ligand-gated ion channel activation in the GABAA and glycine receptors. *Neurosci. Lett. 371*, 230.
(30) Mercado, J., and Czajkowski, C. (2006) Charged Residues in the α1 and β2 Pre-M1 Regions Involved in GABAA Receptor Activation. *J. Neurosci. 26*, 2031.
(31) Fisher, Z., Hernandez Prada, J. A., Tu, C., Duda, D., Yoshioka, C., An, H., Govindasamy, L., Silverman, D. N., and McKenna, R. (2005) Structural and Kinetic Characterization of Active-Site Histidine as a Proton Shuttle in Catalysis by Human Carbonic Anhydrase II. *Biochemistry 44*, 1097−1105.
(32) Mikulski, R., and Silverman, D. (2010) Proton Transfer in Catalysis and the Role of Proton Shuttles in Carbonic Anhydrase. *Biochim. Biophys. Acta, Proteins Proteomics 1804*, 422−426.
(33) Szczot, M., Kisiel, M., Czyzewska, M. M., and Mozrzymas, J. W. (2014) alpha1F64 Residue at GABA(A) receptor binding site is involved in gating by influencing the receptor flipping transitions. *J. Neurosci. 34*, 3193−3209.
(34) Gielen, M. C., Lumb, M. J., and Smart, T. G. (2012) Benzodiazepines modulate GABAA receptors by regulating the preactivation step after GABA binding. *J. Neurosci. 32*, 5707−5715.
(35) Brodzki, M., Rutkowski, R., Jatczak, M., Kisiel, M., Czyzewska, M. M., and Mozrzymas, J. W. (2016) Comparison of kinetic and pharmacological profiles of recombinant α1γ2L and α1β2γ2L GABAA receptors − A clue to the role of intersubunit interactions. *Eur. J. Pharmacol. 784*, 81−89.
(36) Lema, G. M., and Auerbach, A. (2006) Modes and models of GABA(A) receptor gating. *J. Physiol. 572*, 183−200.
(37) Mozrzymas, J. W., Barberis, A., Michalak, K., and Cherubini, E. (1999) Chlorpromazine Inhibits Miniature GABAergic Currents by Reducing the Binding and by Increasing the Unbinding Rate of GABAA Receptors. *J. Neurosci. 19*, 2474.
(38) Mozrzymas, J. W., Wójtowicz, T., Piast, M., Lebida, K., Wyrembek, P., and Mercik, K. (2007) GABA transient sets the susceptibility of mIPSCs to modulation by benzodiazepine receptor agonists in rat hippocampal neurons. *J. Physiol. 585*, 29−46.
(39) Barberis, A., Petrini, E. M., and Mozrzymas, J. W. (2011) Impact of synaptic neurotransmitter concentration time course on the kinetics and pharmacological modulation of inhibitory synaptic currents. *Front. Cell. Neurosci. 5*, 6.
(40) Dietrich, C. J., and Morad, M. (2010) Synaptic Acidification Enhances GABAA Signaling. *J. Neurosci. 30*, 16044.
(41) Xiu, X., Hanek, A. P., Wang, J., Lester, H. A., and Dougherty, D. A. (2005) A unified view of the role of electrostatic interactions in modulating the gating of Cys loop receptors. *J. Biol. Chem. 280*, 41655−41666.
(42) Kash, T. L., Dizon, M. J., Trudell, J. R., and Harrison, N. L. (2004) Charged residues in the beta2 subunit involved in GABAA receptor activation. *J. Biol. Chem. 279*, 4887−4893.
(43) Strickler, S. S., Gribenko, A. V., Gribenko, A. V., Keiffer, T. R., Tomlinson, J., Reihle, T., Loladze, V. V., and Makhatadze, G. I. (2006) Protein Stability and Surface Electrostatics: A Charged Relationship. *Biochemistry 45*, 2761−2766.
(44) Roca, M., Messer, B., and Warshel, A. (2007) Electrostatic contributions to protein stability and folding energy. *FEBS Lett. 581*, 2065−2071.
(45) Gielen, M., Thomas, P., and Smart, T. G. (2015) The desensitization gate of inhibitory Cys-loop receptors. *Nat. Commun. 6*, 6829.
(46) Jatczak-Sliwa, M., Terejko, K., Brodzki, M., Michalowski, M. A., Czyzewska, M. M., Nowicka, J. M., Andrzejczak, A., Srinivasan, R., and Mozrzymas, J. W. (2018) Distinct Modulation of Spontaneous and GABA-Evoked Gating by Flurazepam Shapes Cross-Talk Between Agonist-Free and Liganded GABAA Receptor Activity. *Front. Cell. Neurosci. 12*, 237.
(47) Terejko, K., Michałowski, M. A., Dominik, A., Andrzejczak, A., and Mozrzymas, J. W. (2021) Interaction between GABAA receptor α1 and β2 subunits at the N-terminal peripheral regions is crucial for receptor binding and gating. *Biochem. Pharmacol. 183*, 114338.
(48) Velisetty, P., Chalamalasetti, S. V., and Chakrapani, S. (2014) Structural basis for allosteric coupling at the membrane-protein interface in Gloeobacter violaceus ligand-gated ion channel (GLIC). *J. Biol. Chem. 289*, 3013−3025.
(49) Bocquet, N., Nury, H., Baaden, M., Le Poupon, C., Changeux, J.-P., Delarue, M., and Corringer, P.-J. (2009) X-ray structure of a pentameric ligand-gated ion channel in an apparently open conformation. *Nature 457*, 111−114.
(50) Jonas, P. (1995) Fast Application of Agonists to Isolated Membrane Patches. In *Single-Channel Recording* (Sakmann, B., and Neher, E., Eds.) pp 231−243, Springer, Boston, MA, USA, DOI: 10.1007/978-1-4419-1229-9_10.
(51) Mozrzymas, J. W., Barberis, A., Mercik, K., and Zarnowska, E. D. (2003) Binding Sites, Singly Bound States, and Conformation Coupling Shape GABA-Evoked Currents. *J. Neurophysiol. 89*, 871−883.
(52) Jackson, M. B., Wong, B. S., Morris, C. E., Lecar, H., and Christian, C. N. (1983) Successive openings of the same acetylcholine receptor channel are correlated in open time. *Biophys. J. 42*, 109−114.

https://dx.doi.org/10.1021/acschemneuro.0c00781
ACS Chem. Neurosci. 2021, 12, 562−572